Nuclear Physics B98 (1975) 49–72

A STUDY OF HIGH TRANSVERSE MOMENTUM π^0's AT ISR ENERGIES

K. EGGERT, K.L. GIBONI and W. THOMÉ
III. Physikalisches Institut der Technischen Hochschule, Aachen, Germany

B. BETEV *, P. DARRIULAT, P. DITTMANN, M. HOLDER,
K.T. McDONALD **, H.G. PUGH *** and G. VESZTERGOMBI †
CERN, Geneva, Switzerland

T. MODIS and K. TITTEL
Institut für Hochenergie Physik, Heidelberg, Germany

V. ECKARDT, H.J. GEBAUER, R. MEINKE, O.R. SANDER ††
and P. SEYBOTH
Max Planck Institut für Physik und Astrophysik, Munich, Germany

Received 1 August 1975

We present a study of the transverse momentum spectrum of π^0's produced at c.m. angles $\theta = 90°$ and 53° in pp collisions at $\sqrt{s} = 23.6$, 30.8, 45.1, 53.2, and 62.9 GeV. The experiment was performed with a lead-glass detector. The data can be described with the usual parametrization $p_T^{-n} f(x_T, \theta)$, with $n = 7.2 \pm 0.2$. Comparison between the 90° and 53° data further indicates no appreciable dependence on θ, at least for $x_T < 0.3$. Two-particle inclusive cross sections for π^0's produced alongside are also presented. They are observed to have a dependence upon the transverse momentum of the dipion similar to that of single-particle cross sections and with the same value of n. Two-photon decays of η mesons are observed between 3 and 4 GeV/c transverse momentum with a production cross section half of that of π^0.

1. Introduction

The spectrum of particles produced at large transverse momenta in pp collisions at ISR energies provides an important test for strong interaction theories. The ori-

* On leave from Institute of Nuclear Research, Sofia, Bulgaria.
** Present address: University of Chicago, Ill., USA
*** On leave from University of Maryland, College Park, Md., USA.
† Visiting Scientitist from JINR, Dubna, USSR, on leave from Central Research Institute, Budapest, Hungary.
†† Now at UCLA, Los Angeles, Calif., USA.

ginal measurements of the CERN-Columbia-Rockefeller Collaboration [1] were of the π^0 spectrum at 90° and transverse momenta above 2.5 GeV/c. They showed a yield many orders of magnitude above that expected from the naive extrapolation of the low-momentum spectrum. A large amount of theoretical effort has been devoted to the interpretation of this process in terms of hard collisions involving a small number of proton consistuents. In such models inclusive invariant cross sections are of the form [2]

$$E\frac{\mathrm{d}^3\sigma}{\mathrm{d}p^3} \propto p_{\mathrm{T}}^{-n} f(x_{\mathrm{T}}, \theta)\,. \tag{1}$$

Here E and p are the energy and momentum of the particle produced, θ the production angle, $p_{\mathrm{T}} = p \sin\theta$ the transverse momentum and $x_{\mathrm{T}} = 2p_{\mathrm{T}}/\sqrt{s}$, s being the c.m. energy squared. In the absence of any dimension in the basic scattering process, the power n should be equal to 4. This seems to be already excluded by the data which give n in the region of 8 or above [1,3,4]. Under rather general assumptions, Brodsky and Farrar have shown [5] that n is directly related to the number N of point-like constituents taking an active part in the reaction through the relation $n = 2(N - 2)$.

We have made a study of the spectrum of π^0 produced at c.m. angles $\theta = 90°$ and $\theta = 53°$ in pp collisions at the CERN ISR. The data cover the range $\sqrt{s} = 23.6$ to 62.9 GeV and $p_{\mathrm{T}} = 0.5$ to 8 GeV/c. The study is part of a more extensive investigation in which the charged particles associated with the π^0 are observed in a large streamer chamber detector [6]. The results for associated particles are reported separately [7]. In sect. 2 we describe in some detail the lead-glass Čerenkov detector used in the present work, with particular emphasis on aspects relevant to the measurement of inclusive spectra. In sect. 3 we present an analysis of the data in terms of invariant cross section for π^0 production, but with no attempt at identifying the π^0. Resolved photon pairs are studied in sect. 4, and cross sections for π^0 and η production are obtained in limited ranges of transverse momentum. Sect. 5 is devoted to the study of momentum correlations among neutral pions.

2. The detector

2.1. Configuration

Fig. 1 shows the layout of the intersecting beams and associated equipment. Photons are detected in a lead-glass Čerenkov counter which has been previously described [8]. It consists of 61 hexagonal lead-glass blocks, each of inner diameter 13.6 cm and thickness 32 cm (15 radiation lengths). The blocks are stacked in a hexagonal array of approximate area 1 m^2. The detector is located at a transverse distance of 1.9 m from the mean beam line, on the side of the intersect towards which the c.m. of the colliding protons is moving. Two different geometries were

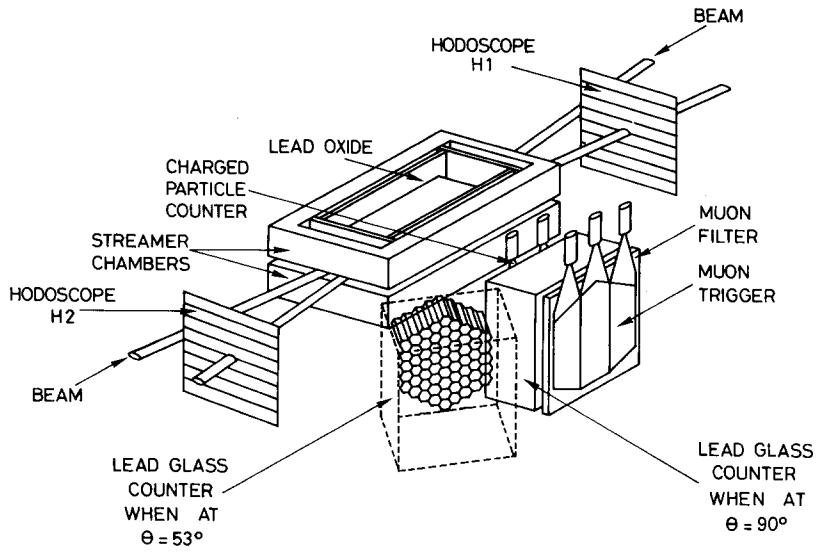

Fig. 1. Layout of the intersecting beams and associated equipment. The lead-glass counter is shown in the $\theta = 90°$ position (full line) and $\theta = 53°$ position (dotted line). In the latter case the phototubes and auxiliary equipment have been omitted to show the details of the lead-glass cell stack.

used, corresponding to mean production angles of 90° and 53° in the c.m. system (fig. 1). The centre of the array is 56 cm below beam plane, corresponding to an average angle of incidence of the photons on the glass of 16°.

The acceptance has the same dependence upon transverse momentum in the 90° and 53° cases, and it covers areas of similar size in the azimuth-rapidity space.

The minimum angle between the decay photons from a π^0 exceeds the diameter of the array for transverse momenta lower than 0.5 GeV/c, and is less than the diameter of a single cell above 3.5 GeV/c. The solid angle covered by the detector in the c.m. system is of the order of 0.3 sr.

2.2. Signal processing

Each lead-glass cell is observed with an EMI 9530 phototube which provides two signals. Anode pulses are analysed in 61 separate 8 bit analogue-to-digital converters (1 channel corresponds to 40 MeV), while dynode pulses are mixed to define an energy threshold. Pedestals are found to be stable within one channel over long periods of time. Anode pulse integration is performed during a 170 nsec gate, covering more than 90% of the pulse area. This gate is generated from the linear sum of all dynode pulses through a discriminator set at very low threshold to avoid time slewing.

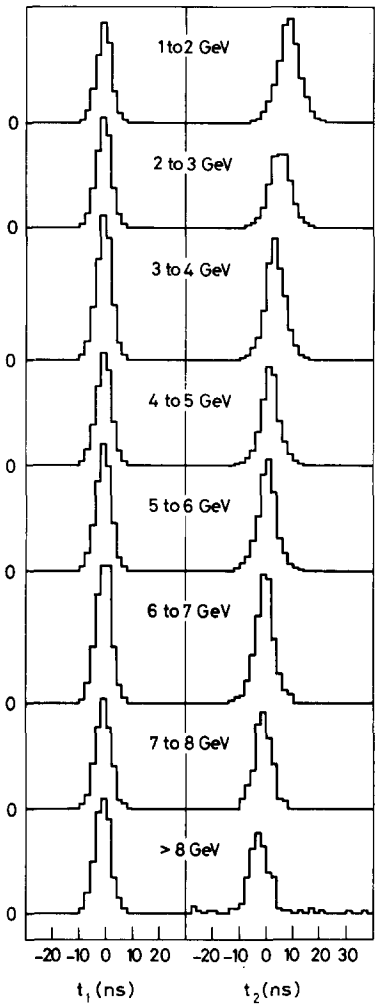

Fig. 2. Time-of-flight distributions between the scintillator hodoscopes of each arm (t_1) and between the lead-glass counter and one of the scintillator hodoscopes (t_2) as a function of the energy of the highest energy cluster detected in the array. In both cases the peaks are well within the resolving times of the corresponding coincidences.

Another discriminator is used to define the threshold above which data are collected.

The data on which cross sections are based are recorded with a trigger which requires a coincidence between the lead-glass signal and signals from both of two large scintillator hodoscopes [9] located on each downstream arm of the intersection

(fig. 1). They see more than 90% of the total inelastic cross section at $\sqrt{s} = 53$ GeV. We have checked that this introduces a negligible bias on the measurement of inclusive cross sections by using the streamer chamber triggered on a pulse in the lead-glass counter, not accompanied by a coincidence between the scintillator hodoscopes.

Time-of-flight spectra of the scintillator hodoscopes and lead-glass Čerenkov signals are continuously recorded, as well as the rates of random coincidences between these signals. Up to the largest transverse momenta, the contamination of random coincidence is negligible (fig. 2).

2.3. Detection of γ rays

The shower produced by a photon is usually well contained in a triplet of adjacent cells [8]. For a γ pair, where the two photons fall in cells separated by at least one cell containing less than 2% of the total π^0 energy, π^0 decays have more than a 50% chance of being resolved pairs between 0.9 and 2.1 GeV/c transverse momentum. Lateral escapes of showers from photons hitting the peripheral cells reduce the effective area of the detector by 15%.

A one radiation length plate, 2 cm thick, made of a lead-oxide araldite mixture, is inserted in the streamer chamber (fig. 1) to observe converted γ rays in its sensitive volume [6]. Its shadow covers most of the lead-glass counter. Two scintillators, tailored to the shape of the lead-glass array and located against its front face, tag events wherein a charged particle or a photon converted in the lead oxide plate enters the counter. Converted photons suffer a small energy loss in the plate. We correct for it by using γ conversion probabilities and electron energy losses [8] obtained in previous measurements.

In a fraction of the events another particle, photon or charged, is detected in the counter in association with the observed π^0. Charged particles deposit an average energy of 400 MeV in the lead glass. When the extra particle is produced at less than 6° to the π^0, it cannot be resolved from it. The apparent energy of the π^0 is then correspondingly increased, and energy spectra have been corrected for this overlap contamination.

For single photons, and because of the good match between cell size and lateral shower development, the impact is located to an accuracy of ± 3 cm, smaller than the cell radius, by using the energy sharing among adjacent cells.

2.4. Energy calibration

The calibration of the energy response of the detector is of central importance in the present work since the spectrum is such a rapidly varying function of p_T. In spite of the presence of 1.5 m thick iron blocks on each side of the detector to provide shielding against radiation, we observed a deterioration of the glass transparency of 30 to 40% over the year during which the experiment was performed. This mostly occurred during beam stacking or at the occasion of machine studies.

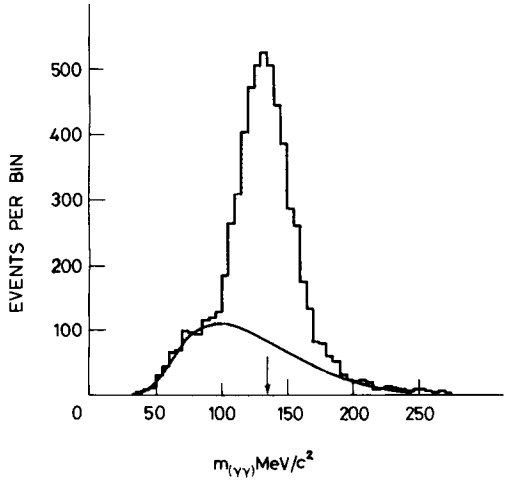

Fig. 3. A typical distribution of the invariant mass of photon pairs with the special π^0 trigger. The curve indicates the background expected from pairs of photons from two different π^0.

Before installation each block had been calibrated in a 1 GeV/c electron beam at the CERN Proton Synchrotron.

A system of light diodes installed on the front face of the lead-glass array was used to maintain the energy calibration throughout the experiment. Each glass cell shares three diodes and each diode illuminates three cells. While the method monitors occasional gain shifts of a few diodes, it does not distinguish between a common gain drop of all cells or of all diodes. In addition, the geometry and frequency spectrum of the light emitted by a diode differ from that of a shower. We have assumed that these difficulties could be ignored. We therefore feel it to be important to check the validity of the energy calibration via other methods, which we briefly mention.

(i) To check the relative cell calibrations we have used a reference light source, made of ^{241}Am imbedded in a small NaI crystal. The method suffers similar geometric and spectral weaknesses as the light diode calibration, but the constancy over time of the light output reference is good.

(ii) Samples of events enriched in π^0 decays with resolved γ pairs have been frequently collected by means of a special trigger mode requiring two nonconverted photons with energies greater than 1 GeV to be observed in the lead-glass detector. Throughout the experiment, the invariant mass distribution of the pairs (fig. 3) is found constant within $\pm 1.5\%$.

(iii) We have used a 10 cm thick iron absorber located behind the counter and followed by scintillators to select events with a muon traversing the glass. For cells traversed over their full length, namely at an angle of less than 15° to the axis of the cell, this permits calibration against the known response to muons [8].

(iv) A further check of the relative calibration of each cell is provided by the distribution of cell population above threshold over the counter area. The method is sensitive to small gain shifts due to the rapid fall-off of the energy spectrum.

The agreement between the various methods is always better than 5%, a figure which we retain as the uncertainty on our energy scale.

A good linearity of the energy response is essential in the present experiment. The phototube response to a light diode was found to deviate from linearity by 2 to 3% at 6 GeV equivalent. A lead-glass cell, equipped with its phototube, has been tested at DESY in an electron beam with energies ranging between 0.5 and 6 GeV. At 6 GeV the response was found to deviate from linearity by about 4%. Bearing in mind that a π^0 of energy E splits into two gammas of energies evenly distributed between 0 and E, the energy deposited in the lead-glass will be correct within 3% up to 8 GeV. Also, since the energy from a single-photon shower is usually deposited in several cells, the phototube non-linearity is unimportant.

The electron beam test at DESY also revealed a non-linearity towards the low-energy end of the response curve. Measured energies were found smaller by approximately 100 MeV below 1 GeV. This observation is confirmed by a comparative study of π^0 and η mass peaks in identical configurations and from the observation of a small dependence of the peak position *versus* energy.

Energies have been corrected for this non-linearity. Lacking sufficient information on its detailed shape towards low energies as well as on its dependence upon glass darkening, an additional uncertainty of ±50 MeV is introduced on the energy scale.

The electron beam test also showed that the energy resolution improves with energy E with a full width at half maximum following approximately the empirical law $\Delta E/E \approx 0.16 - E(\mathrm{GeV})/100$. This form, together with the ±3 cm uncertainty on impact position, accounts well for the observed width of the π^0 mass peak.

3. Invariant cross section for inclusive π^0 production

A total of 7 million events have been recorded, distributed among both production angles and the various c.m. energies available from the CERN ISR. We present an analysis of the data in terms of invariant cross sections for inclusive π^0 production. We assume that contributions other than from π^0 are negligible, an assumption which we shall comment upon later. At higher energies, where the photons from π^0 decays are not resolved, we observe the full π^0 energy. At lower energies we rely on the single-photon spectrum to deduce the transverse momentum distribution of the parent π^0.

For each event, the pattern of energy distribution in the lead-glass array is analysed and reduced to a number of clusters of connected cells with pulse heights significantly above pedestal. Two-photon clusters can be resolved down to a 20 cm separation between photons. On the average an event contains 1.3 clusters, each cluster having more than 90% of its energy in three cells.

Table 1
Invariant cross sections $\mathcal{I} \equiv E(d^3\sigma/dp^3)(\text{mb} \cdot \text{GeV}^{-2} \cdot c^3)$ and the corresponding uncertainties $\Delta\mathcal{I}(\text{mb} \cdot \text{GeV}^{-2} \cdot c^3)$ as a function of transverse momentum p_T (GeV/c) for various values of $\sqrt{s}$ and θ (see sect. 3)

p_T	$\mathcal{I}$	$\Delta\mathcal{I}$	p_T	$\mathcal{I}$	$\Delta\mathcal{I}$
$\sqrt{s}$ = 23.6 GeV, θ = 90°					
0.70	0.823	$0.198 \cdot 10^{-1}$	4.86	$0.314 \cdot 10^{-6}$	$0.687 \cdot 10^{-7}$
0.89	0.222	$0.794 \cdot 10^{-2}$	5.05	$0.293 \cdot 10^{-6}$	$0.624 \cdot 10^{-7}$
1.08	0.103	$0.550 \cdot 10^{-2}$	5.23	$0.137 \cdot 10^{-6}$	$0.436 \cdot 10^{-7}$
1.28	$0.389 \cdot 10^{-1}$	$0.262 \cdot 10^{-2}$	5.41	$0.241 \cdot 10^{-6}$	$0.846 \cdot 10^{-7}$
1.48	$0.158 \cdot 10^{-1}$	$0.130 \cdot 10^{-2}$	5.56	$0.153 \cdot 10^{-6}$	$0.521 \cdot 10^{-7}$
1.69	$0.728 \cdot 10^{-2}$	$0.719 \cdot 10^{-3}$	5.79	$0.718 \cdot 10^{-7}$	$0.367 \cdot 10^{-7}$
1.90	$0.324 \cdot 10^{-2}$	$0.369 \cdot 10^{-3}$			
2.13	$0.130 \cdot 10^{-2}$	$0.147 \cdot 10^{-3}$	$\sqrt{s}$ = 30.8 GeV, θ = 53°		
2.37	$0.507 \cdot 10^{-3}$	$0.556 \cdot 10^{-4}$	0.50	$0.347 \cdot 10^{1}$	$0.821 \cdot 10^{-1}$
2.61	$0.189 \cdot 10^{-3}$	$0.199 \cdot 10^{-4}$	0.68	$0.109 \cdot 10^{1}$	$0.415 \cdot 10^{-1}$
2.85	$0.682 \cdot 10^{-4}$	$0.761 \cdot 10^{-5}$	0.88	0.368	$0.232 \cdot 10^{-1}$
3.08	$0.362 \cdot 10^{-4}$	$0.458 \cdot 10^{-5}$	1.08	0.132	$0.117 \cdot 10^{-1}$
3.32	$0.117 \cdot 10^{-4}$	$0.202 \cdot 10^{-5}$	1.28	$0.452 \cdot 10^{-1}$	$0.513 \cdot 10^{-2}$
3.54	$0.896 \cdot 10^{-5}$	$0.172 \cdot 10^{-5}$	1.50	$0.174 \cdot 10^{-1}$	$0.243 \cdot 10^{-2}$
3.74	$0.379 \cdot 10^{-5}$	$0.102 \cdot 10^{-5}$	1.72	$0.651 \cdot 10^{-2}$	$0.108 \cdot 10^{-2}$
3.90	$0.194 \cdot 10^{-5}$	$0.729 \cdot 10^{-6}$	1.94	$0.301 \cdot 10^{-2}$	$0.557 \cdot 10^{-3}$
4.09	$0.148 \cdot 10^{-5}$	$0.628 \cdot 10^{-6}$	2.17	$0.129 \cdot 10^{-2}$	$0.257 \cdot 10^{-3}$
4.34	$0.308 \cdot 10^{-6}$	$0.301 \cdot 10^{-6}$	2.40	$0.566 \cdot 10^{-3}$	$0.106 \cdot 10^{-3}$
4.48	$0.411 \cdot 10^{-6}$	$0.284 \cdot 10^{-6}$	2.63	$0.261 \cdot 10^{-3}$	$0.465 \cdot 10^{-4}$
			2.85	$0.116 \cdot 10^{-3}$	$0.173 \cdot 10^{-4}$
$\sqrt{s}$ = 30.8 GeV, θ = 90°			3.06	$0.550 \cdot 10^{-4}$	$0.739 \cdot 10^{-5}$
0.70	$0.101 \cdot 10^{1}$	$0.272 \cdot 10^{-1}$	3.26	$0.313 \cdot 10^{-4}$	$0.390 \cdot 10^{-5}$
0.88	0.386	$0.174 \cdot 10^{-1}$	3.46	$0.171 \cdot 10^{-4}$	$0.204 \cdot 10^{-5}$
1.08	0.129	$0.868 \cdot 10^{-2}$	3.65	$0.771 \cdot 10^{-5}$	$0.101 \cdot 10^{-5}$
1.28	$0.430 \cdot 10^{-1}$	$0.384 \cdot 10^{-2}$	3.82	$0.450 \cdot 10^{-5}$	$0.685 \cdot 10^{-6}$
1.48	$0.153 \cdot 10^{-1}$	$0.177 \cdot 10^{-2}$	4.01	$0.219 \cdot 10^{-5}$	$0.420 \cdot 10^{-6}$
1.69	$0.756 \cdot 10^{-2}$	$0.110 \cdot 10^{-2}$	4.19	$0.176 \cdot 10^{-5}$	$0.355 \cdot 10^{-6}$
1.90	$0.340 \cdot 10^{-2}$	$0.589 \cdot 10^{-3}$	4.37	$0.980 \cdot 10^{-6}$	$0.258 \cdot 10^{-6}$
2.13	$0.131 \cdot 10^{-2}$	$0.227 \cdot 10^{-3}$	4.57	$0.519 \cdot 10^{-6}$	$0.173 \cdot 10^{-6}$
2.37	$0.649 \cdot 10^{-3}$	$0.109 \cdot 10^{-3}$	4.75	$0.299 \cdot 10^{-6}$	$0.140 \cdot 10^{-6}$
2.61	$0.295 \cdot 10^{-3}$	$0.447 \cdot 10^{-4}$			
2.85	$0.135 \cdot 10^{-3}$	$0.179 \cdot 10^{-4}$	$\sqrt{s}$ = 45.1 GeV, θ = 90°		
3.09	$0.638 \cdot 10^{-4}$	$0.764 \cdot 10^{-5}$	0.70	$0.123 \cdot 10^{1}$	$0.409 \cdot 10^{-1}$
3.31	$0.298 \cdot 10^{-4}$	$0.319 \cdot 10^{-5}$	0.89	0.400	$0.235 \cdot 10^{-1}$
3.52	$0.168 \cdot 10^{-4}$	$0.169 \cdot 10^{-5}$	1.08	0.144	$0.136 \cdot 10^{-1}$
3.72	$0.875 \cdot 10^{-5}$	$0.855 \cdot 10^{-6}$	1.28	$0.614 \cdot 10^{-1}$	$0.825 \cdot 10^{-2}$
3.92	$0.469 \cdot 10^{-5}$	$0.453 \cdot 10^{-6}$	1.48	$0.240 \cdot 10^{-1}$	$0.433 \cdot 10^{-2}$
4.12	$0.292 \cdot 10^{-5}$	$0.309 \cdot 10^{-6}$	1.69	$0.934 \cdot 10^{-2}$	$0.214 \cdot 10^{-2}$
4.31	$0.135 \cdot 10^{-5}$	$0.169 \cdot 10^{-6}$	1.91	$0.463 \cdot 10^{-2}$	$0.128 \cdot 10^{-2}$
4.49	$0.108 \cdot 10^{-5}$	$0.144 \cdot 10^{-6}$	2.13	$0.219 \cdot 10^{-2}$	$0.615 \cdot 10^{-3}$
4.67	$0.503 \cdot 10^{-6}$	$0.875 \cdot 10^{-7}$			

Table 1 (continued)

2.38	$0.949 \cdot 10^{-3}$	$0.256 \cdot 10^{-3}$
2.62	$0.402 \cdot 10^{-3}$	$0.972 \cdot 10^{-4}$
2.85	$0.218 \cdot 10^{-3}$	$0.460 \cdot 10^{-4}$
3.09	$0.125 \cdot 10^{-3}$	$0.237 \cdot 10^{-4}$
3.31	$0.673 \cdot 10^{-4}$	$0.109 \cdot 10^{-4}$
3.52	$0.399 \cdot 10^{-4}$	$0.581 \cdot 10^{-5}$
3.72	$0.236 \cdot 10^{-4}$	$0.304 \cdot 10^{-5}$
3.92	$0.140 \cdot 10^{-4}$	$0.154 \cdot 10^{-5}$
4.12	$0.880 \cdot 10^{-5}$	$0.932 \cdot 10^{-6}$
4.31	$0.564 \cdot 10^{-5}$	$0.550 \cdot 10^{-6}$
4.49	$0.393 \cdot 10^{-5}$	$0.359 \cdot 10^{-6}$
4.68	$0.274 \cdot 10^{-5}$	$0.235 \cdot 10^{-6}$
4.86	$0.186 \cdot 10^{-5}$	$0.158 \cdot 10^{-6}$
5.04	$0.127 \cdot 10^{-5}$	$0.106 \cdot 10^{-6}$
5.22	$0.978 \cdot 10^{-6}$	$0.821 \cdot 10^{-7}$
5.41	$0.706 \cdot 10^{-6}$	$0.607 \cdot 10^{-7}$
5.59	$0.595 \cdot 10^{-6}$	$0.524 \cdot 10^{-7}$
5.79	$0.373 \cdot 10^{-6}$	$0.371 \cdot 10^{-7}$
5.98	$0.271 \cdot 10^{-6}$	$0.307 \cdot 10^{-7}$
6.21	$0.187 \cdot 10^{-6}$	$0.242 \cdot 10^{-7}$
6.40	$0.116 \cdot 10^{-6}$	$0.190 \cdot 10^{-7}$
6.60	$0.116 \cdot 10^{-6}$	$0.193 \cdot 10^{-7}$
6.80	$0.674 \cdot 10^{-7}$	$0.139 \cdot 10^{-7}$
7.00	$0.672 \cdot 10^{-7}$	$0.145 \cdot 10^{-7}$
7.21	$0.351 \cdot 10^{-7}$	$0.104 \cdot 10^{-7}$
7.39	$0.453 \cdot 10^{-7}$	$0.122 \cdot 10^{-7}$
7.65	$0.238 \cdot 10^{-7}$	$0.818 \cdot 10^{-8}$
7.77	$0.345 \cdot 10^{-7}$	$0.162 \cdot 10^{-7}$
8.02	$0.240 \cdot 10^{-7}$	$0.100 \cdot 10^{-7}$

$\sqrt{s}$ = 45.1 GeV, θ = 53°

0.50	$0.405 \cdot 10^{1}$	$0.987 \cdot 10^{-1}$
0.69	$0.129 \cdot 10^{1}$	$0.511 \cdot 10^{-1}$
0.88	0.454	$0.304 \cdot 10^{-1}$
1.08	0.164	$0.155 \cdot 10^{-1}$
1.28	$0.661 \cdot 10^{-1}$	$0.797 \cdot 10^{-2}$
1.50	$0.276 \cdot 10^{-1}$	$0.399 \cdot 10^{-2}$
1.72	$0.868 \cdot 10^{-2}$	$0.143 \cdot 10^{-2}$
1.94	$0.436 \cdot 10^{-2}$	$0.769 \cdot 10^{-3}$
2.17	$0.201 \cdot 10^{-2}$	$0.360 \cdot 10^{-3}$
2.40	$0.910 \cdot 10^{-3}$	$0.145 \cdot 10^{-3}$
2.63	$0.488 \cdot 10^{-3}$	$0.710 \cdot 10^{-4}$
2.85	$0.241 \cdot 10^{-3}$	$0.281 \cdot 10^{-4}$
3.07	$0.117 \cdot 10^{-3}$	$0.110 \cdot 10^{-4}$
3.27	$0.657 \cdot 10^{-4}$	$0.529 \cdot 10^{-5}$
3.46	$0.408 \cdot 10^{-4}$	$0.287 \cdot 10^{-5}$
3.65	$0.243 \cdot 10^{-4}$	$0.153 \cdot 10^{-5}$
3.83	$0.141 \cdot 10^{-4}$	$0.899 \cdot 10^{-6}$
4.01	$0.886 \cdot 10^{-5}$	$0.601 \cdot 10^{-6}$
4.19	$0.442 \cdot 10^{-5}$	$0.368 \cdot 10^{-6}$
4.39	$0.334 \cdot 10^{-5}$	$0.290 \cdot 10^{-6}$
4.56	$0.218 \cdot 10^{-5}$	$0.228 \cdot 10^{-6}$
4.76	$0.131 \cdot 10^{-5}$	$0.170 \cdot 10^{-6}$
4.94	$0.733 \cdot 10^{-6}$	$0.132 \cdot 10^{-6}$
5.17	$0.570 \cdot 10^{-6}$	$0.106 \cdot 10^{-6}$
5.39	$0.444 \cdot 10^{-6}$	$0.967 \cdot 10^{-7}$
5.57	$0.300 \cdot 10^{-6}$	$0.790 \cdot 10^{-7}$
5.82	$0.203 \cdot 10^{-6}$	$0.675 \cdot 10^{-7}$
6.02	$0.198 \cdot 10^{-6}$	$0.650 \cdot 10^{-7}$
6.22	$0.116 \cdot 10^{-6}$	$0.491 \cdot 10^{-7}$
6.40	$0.124 \cdot 10^{-6}$	$0.124 \cdot 10^{-6}$
6.65	$0.881 \cdot 10^{-7}$	$0.522 \cdot 10^{-7}$

$\sqrt{s}$ = 53.2 GeV, θ = 90°

1.28	$0.732 \cdot 10^{-1}$	$0.126 \cdot 10^{-1}$
1.48	$0.315 \cdot 10^{-1}$	$0.743 \cdot 10^{-2}$
1.69	$0.796 \cdot 10^{-2}$	$0.214 \cdot 10^{-2}$
1.90	$0.498 \cdot 10^{-2}$	$0.167 \cdot 10^{-2}$
2.13	$0.234 \cdot 10^{-2}$	$0.805 \cdot 10^{-3}$
2.37	$0.933 \cdot 10^{-3}$	$0.316 \cdot 10^{-3}$
2.61	$0.439 \cdot 10^{-3}$	$0.137 \cdot 10^{-3}$
2.85	$0.239 \cdot 10^{-3}$	$0.665 \cdot 10^{-4}$
3.09	$0.131 \cdot 10^{-3}$	$0.335 \cdot 10^{-4}$
3.31	$0.732 \cdot 10^{-4}$	$0.165 \cdot 10^{-4}$
3.52	$0.427 \cdot 10^{-4}$	$0.880 \cdot 10^{-5}$
3.72	$0.254 \cdot 10^{-4}$	$0.476 \cdot 10^{-5}$
3.92	$0.151 \cdot 10^{-4}$	$0.245 \cdot 10^{-5}$
4.12	$0.993 \cdot 10^{-5}$	$0.159 \cdot 10^{-5}$
4.31	$0.637 \cdot 10^{-5}$	$0.945 \cdot 10^{-6}$
4.49	$0.436 \cdot 10^{-5}$	$0.609 \cdot 10^{-6}$
4.68	$0.300 \cdot 10^{-5}$	$0.392 \cdot 10^{-6}$
4.86	$0.204 \cdot 10^{-5}$	$0.255 \cdot 10^{-6}$
5.04	$0.157 \cdot 10^{-5}$	$0.189 \cdot 10^{-6}$
5.23	$0.110 \cdot 10^{-5}$	$0.128 \cdot 10^{-6}$
5.41	$0.748 \cdot 10^{-6}$	$0.856 \cdot 10^{-7}$
5.59	$0.535 \cdot 10^{-6}$	$0.617 \cdot 10^{-7}$
5.78	$0.462 \cdot 10^{-6}$	$0.519 \cdot 10^{-7}$
5.98	$0.298 \cdot 10^{-6}$	$0.360 \cdot 10^{-7}$
6.21	$0.223 \cdot 10^{-6}$	$0.287 \cdot 10^{-7}$
6.42	$0.206 \cdot 10^{-6}$	$0.270 \cdot 10^{-7}$
6.60	$0.145 \cdot 10^{-6}$	$0.230 \cdot 10^{-7}$
6.80	$0.900 \cdot 10^{-7}$	$0.167 \cdot 10^{-7}$
7.00	$0.887 \cdot 10^{-7}$	$0.165 \cdot 10^{-7}$
7.21	$0.553 \cdot 10^{-7}$	$0.139 \cdot 10^{-7}$
7.42	$0.610 \cdot 10^{-7}$	$0.140 \cdot 10^{-7}$
7.60	$0.425 \cdot 10^{-7}$	$0.143 \cdot 10^{-7}$

Table 1 (continued)

7.81	$0.365 \cdot 10^{-7}$	$0.115 \cdot 10^{-7}$	7.01	$0.400 \cdot 10^{-7}$	$0.172 \cdot 10^{-7}$
			7.19	$0.462 \cdot 10^{-7}$	$0.179 \cdot 10^{-7}$
$\sqrt{s}$ = 53.2 GeV, θ = 53°					
0.69	$0.150 \cdot 10^{1}$	$0.591 \cdot 10^{-1}$	$\sqrt{s}$ = 62.9 GeV, θ = 90°		
0.88	0.553	$0.368 \cdot 10^{-1}$			
1.08	0.221	$0.206 \cdot 10^{-1}$	0.70	$0.123 \cdot 10^{1}$	$0.473 \cdot 10^{-1}$
1.29	$0.681 \cdot 10^{-1}$	$0.801 \cdot 10^{-2}$	0.89	0.480	$0.351 \cdot 10^{-1}$
1.50	$0.298 \cdot 10^{-1}$	$0.415 \cdot 10^{-2}$	1.08	0.163	$0.194 \cdot 10^{-1}$
1.72	$0.132 \cdot 10^{-1}$	$0.213 \cdot 10^{-2}$	1.28	$0.568 \cdot 10^{-1}$	$0.977 \cdot 10^{-2}$
1.94	$0.550 \cdot 10^{-2}$	$0.926 \cdot 10^{-3}$	1.48	$0.224 \cdot 10^{-1}$	$0.533 \cdot 10^{-2}$
2.18	$0.271 \cdot 10^{-2}$	$0.453 \cdot 10^{-3}$	1.69	$0.965 \cdot 10^{-2}$	$0.299 \cdot 10^{-2}$
2.41	$0.132 \cdot 10^{-2}$	$0.200 \cdot 10^{-3}$	1.90	$0.464 \cdot 10^{-2}$	$0.179 \cdot 10^{-2}$
2.64	$0.726 \cdot 10^{-3}$	$0.996 \cdot 10^{-4}$	2.13	$0.218 \cdot 10^{-2}$	$0.871 \cdot 10^{-3}$
2.86	$0.363 \cdot 10^{-3}$	$0.403 \cdot 10^{-4}$	2.37	$0.109 \cdot 10^{-2}$	$0.435 \cdot 10^{-3}$
3.07	$0.190 \cdot 10^{-3}$	$0.172 \cdot 10^{-4}$	2.61	$0.544 \cdot 10^{-3}$	$0.199 \cdot 10^{-3}$
3.27	$0.107 \cdot 10^{-3}$	$0.815 \cdot 10^{-5}$	2.85	$0.286 \cdot 10^{-3}$	$0.937 \cdot 10^{-4}$
3.46	$0.654 \cdot 10^{-4}$	$0.421 \cdot 10^{-5}$	3.09	$0.157 \cdot 10^{-3}$	$0.472 \cdot 10^{-4}$
3.65	$0.379 \cdot 10^{-4}$	$0.202 \cdot 10^{-5}$	3.31	$0.872 \cdot 10^{-4}$	$0.233 \cdot 10^{-4}$
3.83	$0.240 \cdot 10^{-4}$	$0.113 \cdot 10^{-5}$	3.52	$0.508 \cdot 10^{-4}$	$0.125 \cdot 10^{-4}$
4.01	$0.154 \cdot 10^{-4}$	$0.677 \cdot 10^{-6}$	3.72	$0.302 \cdot 10^{-4}$	$0.682 \cdot 10^{-5}$
4.20	$0.100 \cdot 10^{-4}$	$0.423 \cdot 10^{-6}$	3.92	$0.174 \cdot 10^{-4}$	$0.344 \cdot 10^{-5}$
4.38	$0.659 \cdot 10^{-5}$	$0.280 \cdot 10^{-6}$	4.12	$0.117 \cdot 10^{-4}$	$0.228 \cdot 10^{-5}$
4.57	$0.435 \cdot 10^{-5}$	$0.205 \cdot 10^{-6}$	4.31	$0.740 \cdot 10^{-5}$	$0.136 \cdot 10^{-5}$
4.76	$0.309 \cdot 10^{-5}$	$0.162 \cdot 10^{-6}$	4.49	$0.561 \cdot 10^{-5}$	$0.993 \cdot 10^{-6}$
4.96	$0.206 \cdot 10^{-5}$	$0.124 \cdot 10^{-6}$	4.68	$0.381 \cdot 10^{-5}$	$0.636 \cdot 10^{-6}$
5.16	$0.156 \cdot 10^{-5}$	$0.104 \cdot 10^{-6}$	4.87	$0.261 \cdot 10^{-5}$	$0.444 \cdot 10^{-6}$
5.37	$0.938 \cdot 10^{-6}$	$0.790 \cdot 10^{-7}$	5.04	$0.205 \cdot 10^{-5}$	$0.352 \cdot 10^{-6}$
5.59	$0.582 \cdot 10^{-6}$	$0.601 \cdot 10^{-7}$	5.22	$0.150 \cdot 10^{-5}$	$0.273 \cdot 10^{-6}$
5.81	$0.482 \cdot 10^{-6}$	$0.548 \cdot 10^{-7}$	5.41	$0.131 \cdot 10^{-5}$	$0.236 \cdot 10^{-6}$
6.04	$0.372 \cdot 10^{-6}$	$0.465 \cdot 10^{-7}$	5.59	$0.852 \cdot 10^{-6}$	$0.173 \cdot 10^{-6}$
6.20	$0.315 \cdot 10^{-6}$	$0.438 \cdot 10^{-7}$	5.78	$0.774 \cdot 10^{-6}$	$0.167 \cdot 10^{-6}$
6.41	$0.194 \cdot 10^{-6}$	$0.336 \cdot 10^{-7}$	5.96	$0.520 \cdot 10^{-6}$	$0.127 \cdot 10^{-6}$
6.60	$0.115 \cdot 10^{-6}$	$0.261 \cdot 10^{-7}$	6.22	$0.372 \cdot 10^{-6}$	$0.107 \cdot 10^{-6}$
6.83	$0.928 \cdot 10^{-7}$	$0.232 \cdot 10^{-7}$	6.42	$0.352 \cdot 10^{-6}$	$0.109 \cdot 10^{-6}$

Uncertainties in momentum scale (a 5% calibration uncertainty and a 50 MeV linearity uncertainty) are not included.

In order to enrich the event population towards higher transverse momenta, different energy thresholds were used during data collection, longer times being devoted to higher thresholds. In the vicinity of the threshold this procedure favours events with several photons in the lead-glass counter, each of them with energy below threshold. Such a bias is avoided by considering only events where the highest energy cluster (HEC) is above threshold and produces a trigger by itself.

In order to convert the observed rates from different runs into absolute cross sections, we use as monitor a coincidence between two scintillator telescopes look-

ing at the interaction region at small angles from the downstream proton beams. Monitor rates are free from background and accidental contamination. The monitor has been calibrated to give a measure of ISR luminosity [9]. It sees a cross section rising from 3.0 mb at $\sqrt{s}$ = 23.6 GeV to 15.0 mb at $\sqrt{s}$ = 62.9 GeV. We have checked that data from different runs agree within 4%.

To minimize edge effects, we only retain clusters with less than 80% of their energy contained in outer cells.

A correction is applied to account for chance overlaps with an independent photon or charged particle. It involves the knowledge of the energy spectrum of resolved extra clusters, as well as of the ratio between unresolved overlaps and resolved pairs. The latter is estimated from a sample of fake events built by superimposing the HEC in one event with the extra clusters in another. The correction is usually below 10% and is highest in the 2–3 GeV/c range, where the proximity of the steep low momentum spectrum is most strongly felt.

A model calculation, including geometry as well as effects of finite cell size, energy resolution and shower development, is used to calculate the probability $\mathcal{P}(p_T, p'_T)$

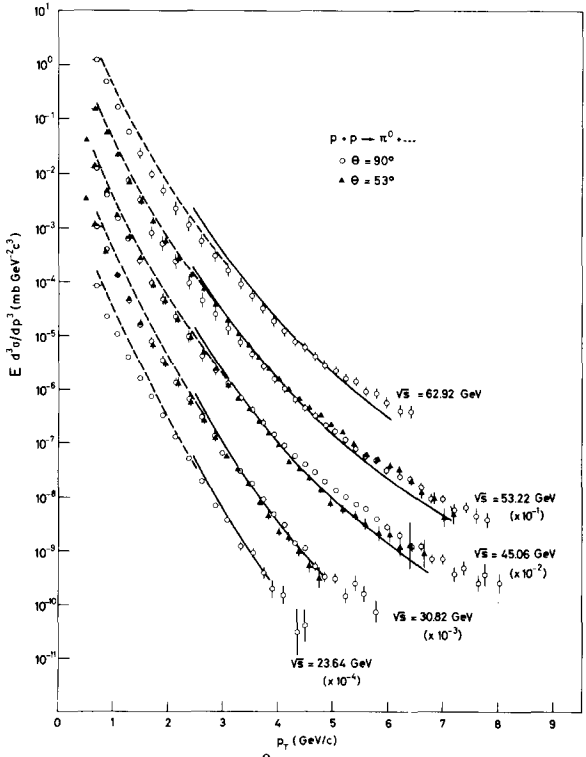

Fig. 4. Inclusive invariant cross sections for π^0 production for various values of θ and $\sqrt{s}$. The solid lines indicate the data of the CERN-Columbia-Rockefeller-Saclay Collaboration [10] and the dashed line those of the British-Scandinavian Collaboration [11].

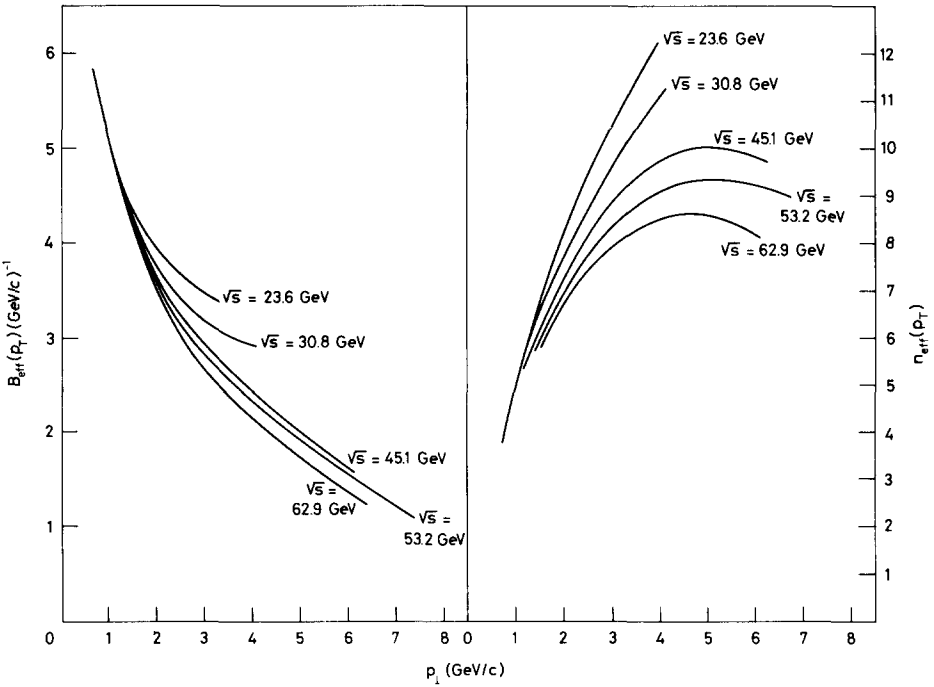

Fig. 5. The local slope $B_{\mathrm{eff}} = -(\mathrm{d}\,\mathcal{I}/\mathcal{I}\,\mathrm{d}p_{\mathrm{T}})$ and local exponent $n_{\mathrm{eff}} = -p_{\mathrm{T}}(\mathrm{d}\,\mathcal{I}/\mathcal{I}\,\mathrm{d}p_{\mathrm{T}})$ as functions of transverse momentum. The curves are smooth lines drawn through the data. Typical error bars are ± 0.5 GeV/c^{-1} for B_{eff} and ± 1 for n_{eff}. The local exponent n_{eff} is not simply related to n in formula (1).

that a π^0 of transverse momentum p_{T} would appear in the detector as an HEC with transverse momentum p'_{T}. This probability function is used to calculate from the HEC spectra the inclusive invariant cross sections $\mathcal{I} = E(\mathrm{d}^3\sigma/\mathrm{d}p^3)$(table 1 and fig. 4) as functions of transverse momentum p_{T}. In addition to statistical uncertainties, errors include systematic effects in overlap corrections and acceptance calculation. Systematic uncertainties of ±5% and, in addition, of ±50 MeV/c must be applied to the momentum scale as discussed above.

Within systematic uncertainties, fair agreement is observed with the CERN-Columbia-Rockefeller-Saclay 90° data [10] * of π^0 production above 2.5 GeV/c. The present data are systematically lower than those of the British-Scandinavian Collaboration [11] of $\pi^{\pm}$ production below 4 GeV/c.

The invariant cross sections exhibit several features which confirm previous observations [1,11].

(i) The expression $\mathcal{I} \propto \mathrm{e}^{-Bp_{\mathrm{T}}}$ is inadequate: this is illustrated in fig. 5a, which

* We thank this Collaboration for having provided us with these data prior to publication.

shows the logarithmic derivative $B_{\text{eff}} = -(1/\mathcal{I})(\mathrm{d}\mathcal{I}/\mathrm{d}p_{\mathrm{T}})$ as a function of transverse momentum. This drops sharply from 6 $(\mathrm{GeV}/c)^{-1}$ to 1.5 $(\mathrm{GeV}/c)^{-1}$ or less.

(ii) The expression $\mathcal{I} \propto p_{\mathrm{T}}^{-n}$ has a limited range of usefulness at p_{T} above 3 GeV/c and at the higher values of $\sqrt{s}$. This is illustrated in fig. 5b, which shows the local exponent $n_{\text{eff}} = -(p_{\mathrm{T}}/\mathcal{I})(\mathrm{d}\mathcal{I}/\mathrm{d}p_{\mathrm{T}})$ as a function of transverse momentum. The exponent levels off at about 10 for high transverse momentum, but it is clear that a simple power law dependence is generally inadequate.

(iii) At fixed s, invariant cross sections, when expressed as functions of p_{T} and θ, are independent of production angle within errors. This observation had previously been made at lower transverse momenta for charged particles [11]. It now appears to be valid for π^0 production up to $p_{\mathrm{T}} \approx 7$ GeV/c.

In the framework of hard scattering models it is relevant to comment on the adequacy of a form

$$\mathcal{I} = p_{\mathrm{T}}^{-n} f(x_{\mathrm{T}}, \theta) . \tag{1}$$

This is best investigated by displaying contour lines of equal cross sections in the $\{\log x_{\mathrm{T}}, \log p_{\mathrm{T}}\}$ plane. For two such neighbouring lines, corresponding to cross

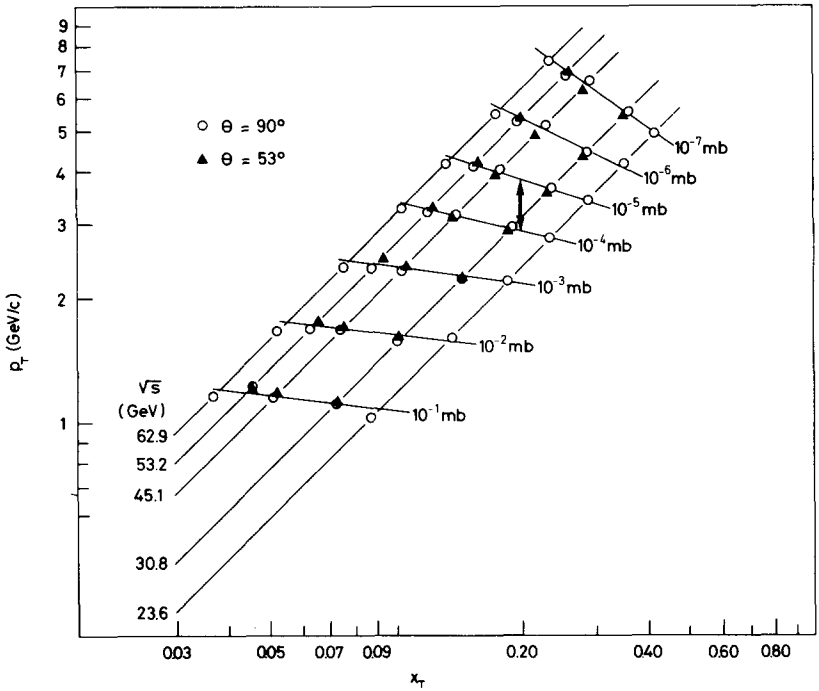

Fig. 6. Lines of constant cross section in the $(\log x_{\mathrm{T}}, \log p_{\mathrm{T}})$ plane. The arrow indicates the spacing corresponding to $n = 8$ (see text).

sections in the ratio 1 : 10, we have at any fixed x_T and θ

$$10 = \frac{\mathcal{G}_1}{\mathcal{G}_2} = \left(\frac{p_{T_2}}{p_{T_1}}\right)^n ,$$

$$\log(p_{T_2}) - \log(p_{T_1}) = \frac{\log 10}{n} .$$

Namely, if eq. (1) applies, lines of equal cross sections are equally spaced in the $(\log x_T, \log p_T)$ plane and their spacing is a direct measure of $1/n$ (fig. 6).

It is indeed found that this is approximately the case in the domain observed, with n of the order of 8, in agreement with previous observations [1]. Towards higher values of x_T the lines tend to become closer together, in qualitative agreement with the higher n value reported at FNAL [3,4]. In order to obtain an average value of n we have used a parametrization,

$$f(x_T, \theta) = A(\theta) \exp[-B(\theta)x_T + C(\theta)x_T^2] .$$

We find that $n = 7.2 \pm 0.2$, when we restrict ourselves to transverse momenta larger than 2 GeV/c. The variation of n seen in fig. 6 shows that one must be cautious before drawing definite conclusions concerning the interpretation of n as re-

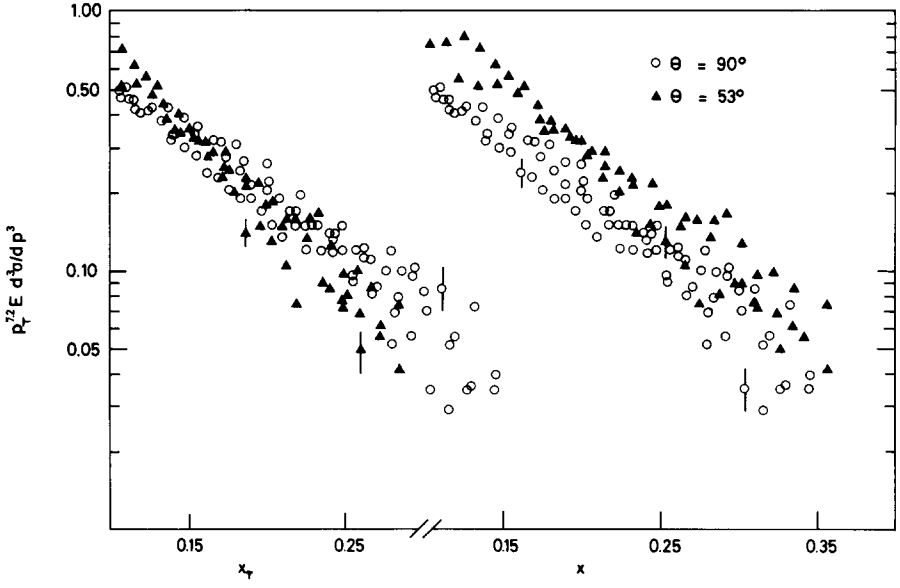

Fig. 7. The expression $p_T^{7.2} E\, d^3\sigma/dp^3$ displayed for $\theta = 90°$ and $\theta = 53°$ *versus* x_T (left side) and x (right side). A few typical error bars are indicated.

lated to the number of constituents taking part in the basic hard scattering process [5]. In the ISR energy range several such processes may still be at play.

We lastly comment on the angular dependence of the invariant cross sections. It has been previously argued by a group at FNAL that $f(x_T, \theta)$ depends upon the single variable $x = x_T/\sin\theta$ only [12]. This might still be compatible with $\mathcal{D}$ being observed, within errors, to be independent of angle, because $\mathcal{D}$ is dominated by the factor p_T^{-n}, and $f(x_T, \theta)$ only accounts for smaller variations with θ and $\sqrt{s}$. To study this question in more detail, we compare the dependence of $p^{7.2}\,\mathcal{D}$ upon x_T and x in figs. 7a and 7b, respectively. In the range of the present experiment ($x < 0.3$) our data exclude that $f(x_T, \theta)$ would be a function of the single parameter x.

4. Resolved photon pairs

Between 1 and 2 GeV/c transverse momentum, π^0 decays can be identified from the invariant mass of resolved photon pairs. This is the range where the opening angle of the photons is smaller than the angular aperture of the lead-glass array, but large enough to produce separated energy clusters. Similarly, two-photon decays of η mesons (branching ratio (38 ± 1)% [13]) can be detected above 3 GeV/c transverse momentum. The acceptance of the detector is, however, not sufficient to detect $\omega \to \pi^0\gamma$ decays.

We have analysed the data in terms of invariant cross sections for identified photon pairs. Data reduction proceeds as described in the preceding section. The threshold bias cut is now applied to the energy of the pair rather than that of the HEC. Overlap corrections are less important because they modify the value of the invariant mass and cause a small loss of events rather than shifting the spectrum to higher p_T values. We have checked that the asymmetry $A = (\epsilon_2 - \epsilon_1)/(\epsilon_2 + \epsilon_1)$ between two photons of energies ϵ_2 and ϵ_1, and with an invariant mass consistent with the π^0 mass, is flat. We require that $|A|$ be less than 0.4 to restrict the data to a region where the acceptance can be calculated with maximum reliability. We perform a background subtraction, which accounts for photon pairs from two different π^0's and amounts to approximately 60% near p_T = 1 GeV/c and 20% near p_T = 2 GeV/c. Thirty per cent of this subtraction is added to the final error in quadrature. We then obtain invariant cross sections for π^0 production which are compared in fig. 8 with those of sect. 3. The present results are usually lower, on the average by 30%. The low-energy non-linearity of the detector affects the two analyses in different ways. In the former it applies to a single photon carrying most of the π^0 momentum, in the latter it applies to each of the two photons which share the π^0 momentum rather evenly. For example, both analyses would yield similar cross sections if the momenta were additionally increased by 70 MeV/c. This would also bring the data in closer agreement with π^- cross sections below 3 GeV/c [11].

If the 30% average difference between the present analysis and that of sect. 3 is

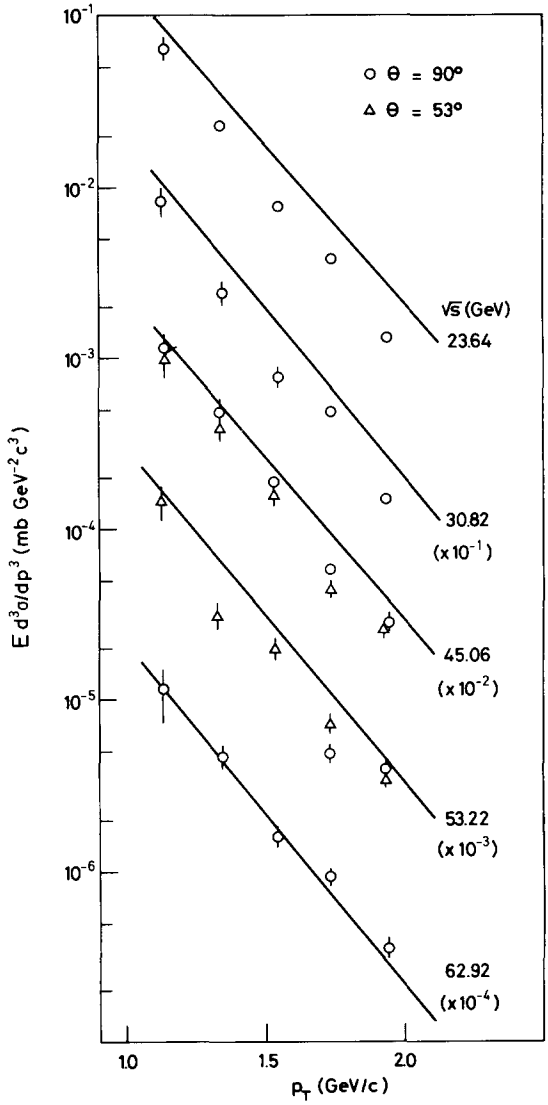

Fig. 8. Invariant cross sections for inclusive π^0 production calculated from observed $\pi^0 \to \gamma\gamma$ decays. The lines indicate the results of the analysis using energy clusters.

attributed to η production, we find that the invariant cross sections for inclusive productions of η and π^0 mesons should be in the ratio 0.63 : 1.

Photon pairs from η decays are detected in an energy range where the performance of the detector is more reliable. They exhibit a clear peak around the η mass,

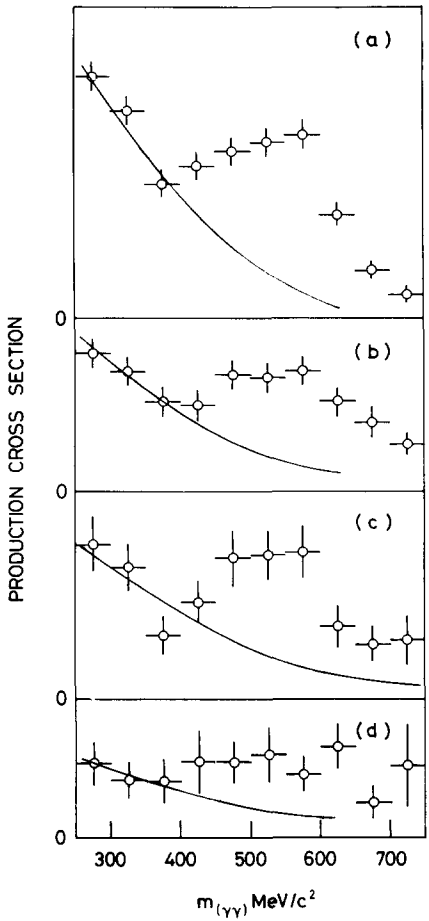

Fig. 9. Invariant mass distribution of photon pairs produced at $\theta = 90°$ and $\sqrt{s} = 53.2$ GeV for different intervals of the pair transverse momentum; (a) 3 to 3.5 GeV/c, (b) 3.5 to 4 GeV/c, (c) 4 to 4.5 GeV/c, (d) 4.5 to 5 GeV/c. The lines indicate the contribution from uncorrelated pairs.

however above a substantial background (fig. 9). The data at $\sqrt{s} = 53.2$ GeV and $\theta = 90°$ are the only ones with sufficient statistics to permit such an analysis. Invariant cross sections are displayed in fig. 10 and listed in table 2. Errors include statistical incertainties and 30% of the background subtraction added in quadrature. Over the small range of transverse momentum explored (3 to 4.5 GeV/c) the cross section has a momentum dependence similar to that of the π^0's and a magnitude half as large, in agreement with previously reported results [14].

Under the assumption, for which we have no evidence, that η and π^0 cross sections are in the ratio 1 : 2 over the full momentum range, the π^0 cross sections of

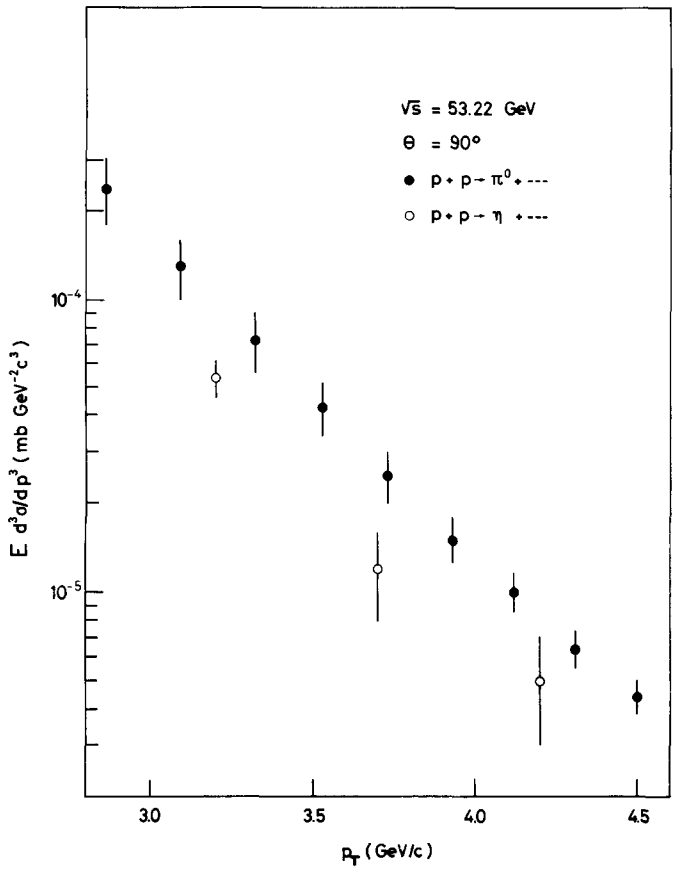

Fig. 10. Invariant cross sections at $\sqrt{s}$ = 53.2 GeV and θ = 90° for η and π^0 production between 3.0 and 4.5 GeV/c transverse momentum.

Table 2
Invariant cross section for η inclusive production at θ = 90°, $\sqrt{s}$ = 53.2 GeV

p_T (GeV/c)	$\vartheta\eta$ (mb · GeV^{-2} · c^3)
3.2	(5.4 ± 0.8) × 10^{-5}
3.7	(1.2 ± 0.4) × 10^{-5}
4.2	(0.5 ± 0.2) × 10^{-5}

the preceding section should be multiplied by a correction factor of the form $1 - \epsilon(p_T)$, where $\epsilon(p_T)$ decreases exponentially from 30% at 1 GeV/c to 3% at 5 GeV/c.

5. Momentum correlations among neutral pions

We now consider events with two neutral pions detected in the lead-glass array. Such events provide information on momentum correlations among neutral pions produced alongside within the small angular acceptance (0.3 sr) of the detector.

Data reduction proceeds along similar lines as before. We select events with at least two energy clusters, of which at least one is above threshold. We apply no constraint on energy asymmetry, but require the energy clusters of the two π^0 to be more than two cell diameters apart. Contributions of two photon decays from a single π^0 or η are subtracted with the assumption that η and π^0 cross sections are in

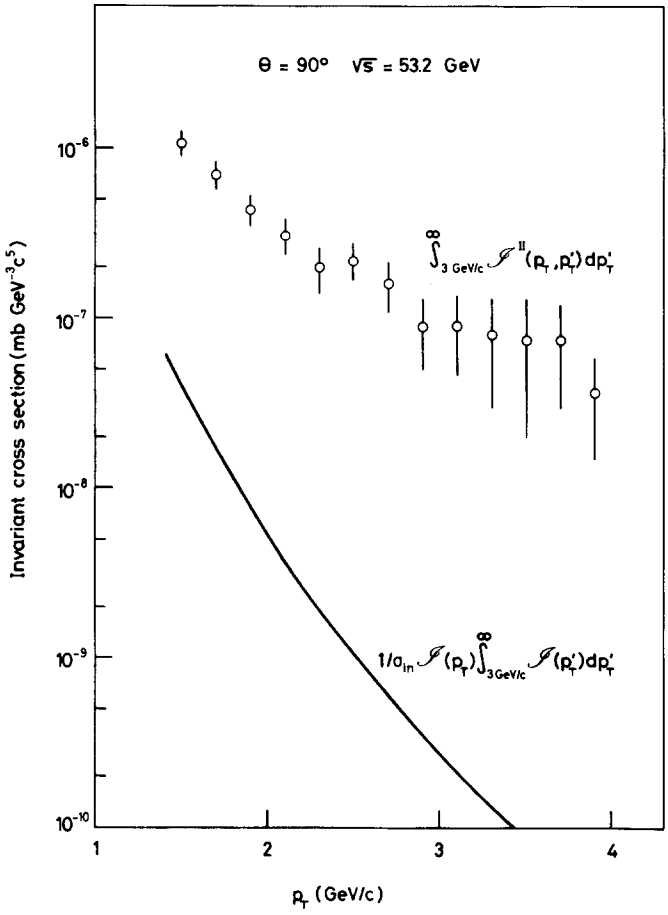

Fig. 11. Two-particle invariant cross section integrated over transverse momenta larger than 3 GeV/c of one of the pions. The lines indicate which values this quantity would take in the absence of correlation.

the ratio 1 : 2 everywhere. The knowledge of the acceptance of the detector to detect a π^0 as a single energy cluster corresponding either to one or to both decay photons is used to reduce the data to two-particle invariant cross sections and to study their dependence upon the π^0 transverse momenta p_T and p'_T,

$$\mathcal{I}^{II}(p_T, p'_T) = EE' \frac{d^6\sigma}{d^3p d^3p'} .$$

Statistics are not sufficient to conveniently display $\mathcal{I}^{II}(p_T, p'_T)$ in two dimensions. We first illustrate the main features of the dependence of $\mathcal{I}^{II}$ over p_T and p'_T by requiring one of the particles to have a transverse momentum $p'_T > 3$ GeV/c and looking at the transverse momentum distribution of the other. To this effect, we compare

$$\mathcal{I}^{II}_{corr} = \int_{3\,GeV/c}^{\infty} \mathcal{I}^{II}(p_T, p'_T) dp'_T$$

to the uncorrelated equivalent

$$\mathcal{I}^{II}_{unc} = \frac{I}{\sigma_{in}} \mathcal{I}(p_T) \int_{3\,GeV/c}^{\infty} \mathcal{I}(p'_T) dp'_T ,$$

where σ_{in} is the inelastic pp cross section.

These cross sections are displayed in fig. 11 for $\theta = 90°$ and $\sqrt{s} = 53.2$ GeV. We observe a strong positive correlation, increasing with p_T and p'_T. The ratio $R = \mathcal{I}^{II}_{corr}/\mathcal{I}^{II}_{unc}$ is of the order of 100 at $p'_T \sim 3$ GeV/c, in agreement with previous observations from the CERN-Columbia-Rockefeller Collaboration [15]. The situation is very similar to that observed for correlations between neutral pions and charged hadrons [16]. It should be remarked that the very large values taken by the correlation coefficient R partly reflect the rapid decrease of the single-particle inclusive yields with p_T. The existence of such a strong correlation is nonetheless of central importance in understanding the dynamics underlying large transverse momentum processes. Apart for the η's, which have been subtracted in the analysis, the invariant mass distribution of the pairs shows no structure within the range explored here (0.2 to 1.0 GeV/c^2). This excludes that the correlation arise from a 2γ decay of some large transverse momentum object with definite mass. Simple constituent interchange models [17], which describe successfully single-particle cross sections, fail to predict such large correlations [18]. The $K_s \to 2\pi^0$ decays are a possible source of correlations. Depending upon the momentum range and the decay configuration, a part or all of the four decay photons may be resolved and detected. Unless each π^0 produces a single-energy cluster in the lead-glass counter, the invariant mass of a cluster pair will be lower than that of the K^0. We have calculated the contribution to $\mathcal{I}^{II}$ of this process under the assumption that K_s and π^0 were produced

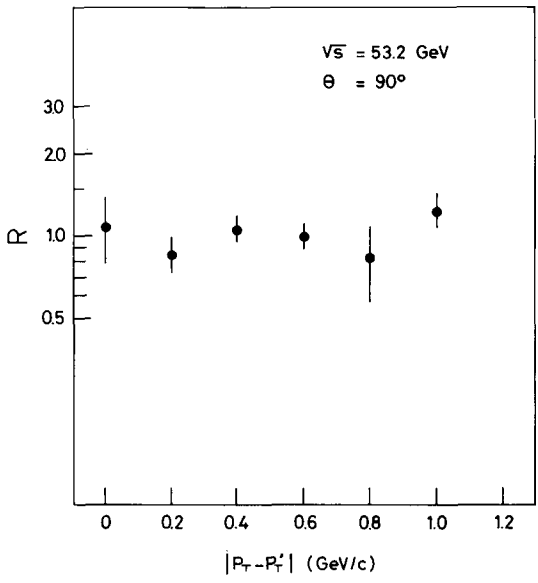

Fig. 12. In order to illustrate the independence of the two-particle cross section upon $p_T - p'_T$, we have divided the invariant cross section at the point (p_T, p'_T) by its average over $p_T - p'_T$ at fixed $p_T + p'_T$. The result was found not to depend significantly upon $p_T + p'_T$ and its average value R is displayed *versus* $|p_T - p'_T|$.

in the ratio 1 : 2. It is found to decrease from ~10% at $p_T + p'_T = 3$ GeV/c to ~3% at $p_T + p'_T = 7$ GeV/c. The data are not corrected for this effect.

It is instructive to study the dependence of $\mathcal{I}^{II}(p_T, p'_T)$ over the total transverse momentum of the dipion, $\tilde{p}_T \approx p_T + p'_T$. This is justified by the fact that $\mathcal{I}^{II}$ is observed (fig. 12) to be only weakly dependent upon $p_T - p'_T$. In addition, if both particles are "children" of a same "parent", $p_T + p'_T$ is the transverse momentum produced in the solid angle of the detector, the analogue of p_T in the single-particle case *. To this effect we average $\mathcal{I}^{II}(p_T, p'_T)$ at fixed $p_T + p'_T$ over $p_T - p'_T$, limiting each transverse momentum above 1 GeV/c to avoid important corrections from $\pi^0 \to \gamma\gamma$ decays. The results are displayed in fig. 13 and show a striking resemblance to the single-particle cross sections. In particular, $\langle \mathcal{I}^{II}(p_T, p'_T) \rangle$ is observed not to depend upon θ within errors.

In analogy with the single-particle case, we have attempted to describe data with a form

$$\langle \mathcal{I}^{II} \rangle = A(p_T + p'_T)^{-n} \exp[-B(x_T + x'_T)] \ .$$

* The relevance of displaying correlations as a function of $p_T + p'_T$ was first pointed out to one of us by J.D. Bjorken.

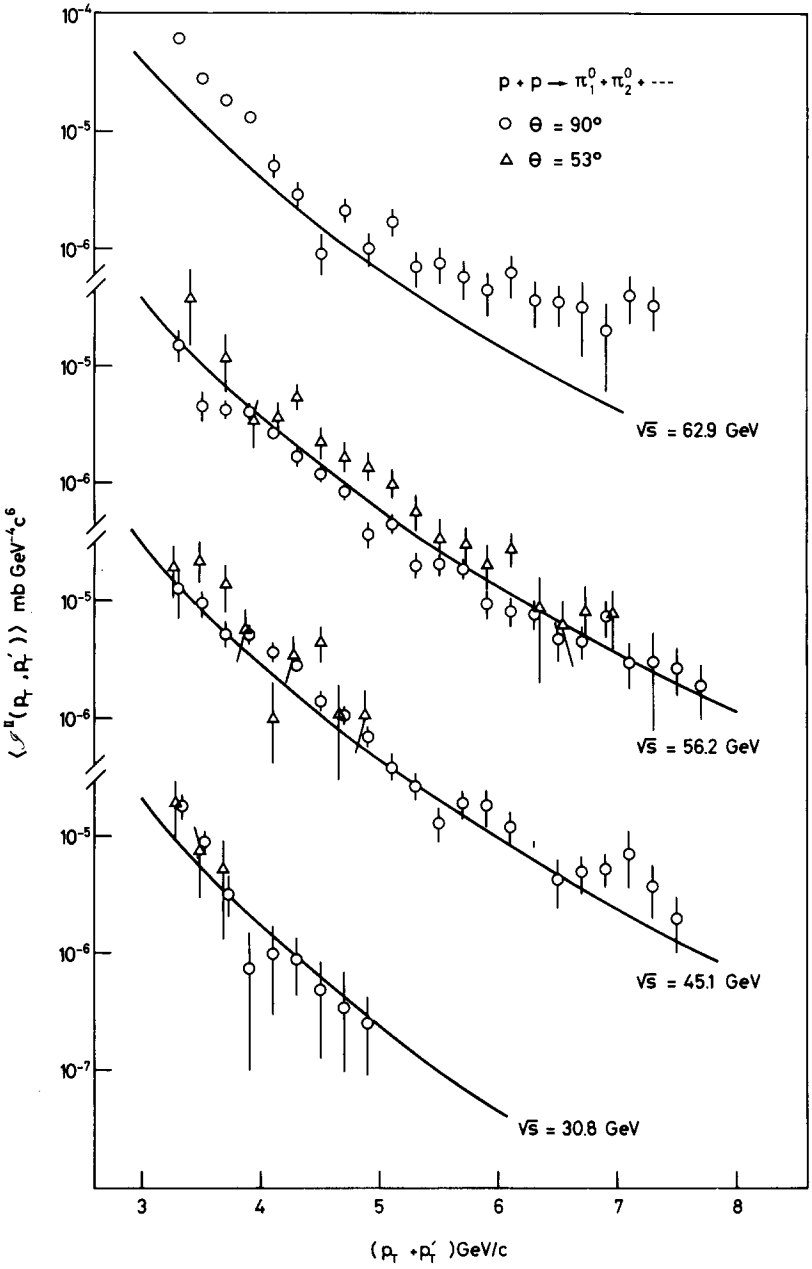

Fig. 13. Two-particle invariant cross sections for inclusive production of two π^0, averaged over the difference between their transverse momenta $p_T - p'_T$. The data are displayed *versus* the sum $p_T + p'_T$ of the π^0 transverse momenta. The lines indicate the result of the fit to the expression $A(p_T + p'_T)^{-n} \exp[-B(x_T + x'_T)]$ with $n = 7.1 \pm 0.5$.

The best fit is obtained with $n = 7.1 \pm 0.5$ ($p_T + p'_T > 3.4$ GeV/c) exactly as for single-particle cross sections. The agreement with the data at $\sqrt{s} = 62.9$ GeV is however poor (fig. 13) and B takes a smaller value than in the single-particle case.

6. Conclusion

We have taken advantage of the large solid angle coverage of our lead-glass detector to study high transverse momentum production of neutral pions at ISR energies. Our data confirm and extend previous measurements of single-particle and two-particle inclusive spectra:

(i) invariant cross sections follow approximately a $p_T^{-n} f(x_T, \theta)$ law for transverse momenta above ≈ 2 GeV/c with $n = 7.2 \pm 0.2$. But we have shown, by presenting our data in the $(\log p_T, \log x_T)$ plane, that there is no clear evidence for a single value of n describing the data over the whole ISR energy range;

(ii) the scaling function $f(x_T, \theta)$ shows no appreciable dependence upon θ in the range $\theta = 53° - 90°$, $x_T < 0.3$;

(iii) two-particle inclusive cross sections show very similar properties, when expressed as functions of the transverse momentum of the dipion, to that of single-particle inclusive cross sections. Such correlations are stronger than expected from simple constituent interchange models;

(iv) we have observed $\eta \to \gamma\gamma$ decays between 3 and 4.5 GeV/c transverse momentum. The η production cross section is about half that of π^0.

Identification of $\pi^0 \to \gamma\gamma$ decays was only possible between 1 and 2 GeV/c transverse momentum. Above this range, we have, in principle, no assurance that we indeed observed π^0's.

We wish to thank Professors H. Faissner and N. Schmitz for their support, Professor C. Rubbia and his colleagues of the Aachen-CERN-Torino Collaboration, with whom the lead-glass detector was designed, constructed, and used in a previous experiment, Drs. P. Joss and F. Peters for invaluable help during the energy calibration measurements at DESY, Messrs. L. Bonnefoy and J.M. Chapuis for technical assistance and Mrs. M. Ferigoule for help in the data analysis.

We have benefited from several instructive discussions with Professors A.P. Contogouris, G. Farrar, M. Jacob, and our colleagues of the CERN-Columbia-Rockefeller Collaboration.

Partial financial support was given by the Bundesministerium für Forschung und Technologie.

References

[1] F.W. Büsser, L. Camillari, L. di Lella, G. Gladding, A. Placci, B.G. Pope, A.M. Smith, J.K. Yoh, E. Zavattini, B.J. Blumenfeld, L.M. Lederman, R.L. Cool, L. Litt and S.L. Segler, Phys. Letters 46B (1973) 471.

[2] S.M. Berman and M. Jacob, Phys. Rev. Letters 25 (1970) 1683;
S.M. Berman, J.D. Bjorken and J.B. Kogut, Phys. Rev. D4 (1971) 3388;
J.D. Bjorken, Proc. 2nd Int. Conf. on elementary particles, Aix-en-Provence, 1973; J. de Phys. 34 Suppl. 10 (1973) 385;
P.V. Landshoff, Proc. 17th Int. Conf. on high-energy physics, London, 1974 (Rutherford Lab., Chilton, Didcot, 1974) p. V-57.
[3] J. Cronin, H. Frisch, M. Schohet, J. Boymond, P. Piroué and R. Summer, Phys. Rev. Letters 31 (1973) 1426.
[4] D. Carey, M. Goldberg, J. Johnson, D. Ritchie, A. Roberts, R. Shofer, D. Theriot, E. von Goeler, J. Walker, M. Wong and F. Taylor, Phys. Rev. Letters 32 (1974) 24.
[5] S.J. Brodsky and G.R. Farrar, Phys. Rev. Letters 31 (1973) 1153; Phys. Rev. D11 (1975) 1309.
[6] K. Eggert, W. Thomé, B. Betev, G. Bohm, P. Darriulat, P. Dittmann, E. Gygi, M. Holder, K.T. McDonald, T. Modis, H.G. Pugh, F. Schneider, H. Albrecht, K. Tittel, I. Derado, V. Eckardt, H.J. Gebauer, R. Meinke, O.R. Sander and P. Seyboth, Nucl. Instr. 126 (1975) 477.
[7] K. Eggert, K.L. Giboni, W. Thomé, B. Betev, P. Darriulat, P. Dittman, M. Holder, J. Kaltwasser, K.T. McDonald, T. Modis, H.G. Pugh, G.J. Vesztergombi, K. Tittel, P. Allen, I. Derado, V. Eckardt, H.J. Gebauer, R. Meinke, O.R. Sander, P. Seyboth and S. Uhlig, Nucl. Phys. B98 (1975) 73.
[8] M. Holder, E. Radermacher, A. Staude, P. Darriulat, J. Deutsch, J. Pilcher, C. Rubbia, K. Tittel, C. Grosso-Pilcher, M. Scire and A. Villari, Nucl. Instr. 108 (1973) 541; P. Darruilat, E. Gygi, M. Holder, K.T. McDonald, H.G. Pugh, F. Schneider and K. Tittel, Conversion efficiency of lead for 30–200 MeV photons, submitted to Nucl. Instr.
[9] K. Eggert, H. Frenzel, K.L. Giboni, W. Thomé, B. Betev, P. Darriulat, P. Dittmann, M. Holder, K.T. McDonald, T. Modis, H.G. Pugh, K. Tittel, V. Eckardt, H.J. Gebauer, R. Meinke, O.R. Sander and P. Seyboth, Nucl. Phys. B98 (1975) 93.
[10] F.W. Büsser et al., to be published.
[11] B. Alper, H. Bøggild, P. Booth, L.J. Carroll, G. von Dardel, G. Damgaard, B. Duff, J.N. Jackson, G. Jarlskog, L. Jönsson, A. Klovning, L. Leistam, E. Lillethun, S. Olgaard-Nielsen, M. Prentice and J.M. Weiss, Nucl. Phys. B87 (1975) 19.
[12] D.C. Carey, J.R. Johnson, R. Kammerud, M. Petters, D.J. Ritchie, A. Roberts, J.R. Sauer, R. Shafer, D. Theriot, J.K. Walker and F.E. Taylor, Phys. Rev. Letters 33 (1974) 327, 330.
[13] Particle Data Group, Phys. Letters 50B (1974) 61.
[14] F.W. Büsser, L. Camilleri, L. di Lella, B.G. Pope, A.M. Smith, B.J. Blumenfeld, S.N. White, A.F. Rothenberg, S.L. Segler, M.J. Tannenbaum, M. Banner, J.B. Chèze, H. Kasha, J.P. Pansart, G. Smadja, J. Teiger, H. Zaccone and A. Zylberstejn, Phys. Letters B55 (1975) 232.
[15] F.W. Büsser, L. Camilleri, L. di Lella, B.G. Pope, A.M. Smith, J.K. Yoh, B.J. Blumenfeld, L.M. Lederman, R.L. Cool, L. Litt and S.L. Segler, Phys. Letters 51B (1974) 311.
[16] CERN-Columbia-Rockefeller-Saclay Collaboration, Proc. 17th Int. Conf. on high-energy physics, London, 1974 (Rutherford Lab., Chilton, Didcot, 1974) p. V-13.
[17] R. Blankenbecler, S.J. Brodsky and J.F. Gunion, Phys. Letters 39B (1972) 649; 42B (1973) 461; Phys. Rev. D6 (1972) 2652; D8 (1973) 287.
[18] D. Schiff, A.P. Contogouris and J.L. Alonso, Phys. Letters 55B (1975) 87.